Custom 3D Printed Spatial Atomic Layer Deposition Manifold for the Coating of Tubular Membranes

Fidel Toldra-Reig, Clément Lausecker, Matthieu Weber, Mikhael Bechelany, David Muñoz-Rojas

► To cite this version:

Fidel Toldra-Reig, Clément Lausecker, Matthieu Weber, Mikhael Bechelany, David Muñoz-Rojas. Custom 3D Printed Spatial Atomic Layer Deposition Manifold for the Coating of Tubular Membranes. ACS Sustainable Chemistry & Engineering, 2022, 10 (43), pp.14112-14118. 10.1021/acssuschemeng.2c04424 . hal-03852184

HAL Id: hal-03852184
https://hal.umontpellier.fr/hal-03852184v1

Submitted on 14 Nov 2022

HAL is a multi-disciplinary open access archive for the deposit and dissemination of scientific research documents, whether they are published or not. The documents may come from teaching and research institutions in France or abroad, or from public or private research centers.

L'archive ouverte pluridisciplinaire **HAL**, est destinée au dépôt et à la diffusion de documents scientifiques de niveau recherche, publiés ou non, émanant des établissements d'enseignement et de recherche français ou étrangers, des laboratoires publics ou privés.

Custom 3D Printed Spatial Atomic Layer Deposition Manifold for the Coating of Tubular Membranes

Fidel Toldra-Reig [a,†,], Clément Lausecker [a,b], Matthieu Weber [a], Mikhael Bechelany [b] and David Muñoz-Rojas [a,**]*

[a] Univ. Grenoble Alpes, CNRS, Grenoble INP, LMGP, F-38000 Grenoble, France
[b] Institut Européen des Membranes, IEM, UMR-5635, Univ. Montpellier, CNRS, ENSCM, Place Eugène Bataillon 34095 Montpellier cedex 5, France

Abstract

The development of highly efficient membranes represents a great opportunity to significantly reduce the environmental impacts of human activities through gas separation and water filtration, and are also very attractive for process intensification when coupled to existing industrial processes. Tubular membranes have higher modularity, better pressure resistance, and they offer easier sealing than their flat counterparts. The ability to deposit thin films on their surface is crucial to optimize their chemical and physical properties. However, the deposition of thin films on tubular membrane supports with conventional vacuum-based deposition techniques is relatively complex, slow and costly. In this work the versatility of spatial atomic layer deposition (SALD) and 3D printing technologies has been combined to design and fabricate a custom SALD manifold for coating tubular substrates. SALD is a scalable deposition technique, offering high-throughput at atmospheric pressure and thus can be advantageously employed to coat tubular membranes, enabling high quality thin films to be deposited at the nanoscale considerably faster than with other conventional techniques. Computational fluid dynamics (CFD) calculations by means of COMSOL Multiphysics have been used to optimize this innovative SALD gas manifold. The proof-of-concept of the new SALD manifold has been validated through successful ZnO thin film depositions performed on tubular Cu foils and porous Al2O3 tubular membrane supports, demonstrating the capability of SALD to achieve high-throughput depositions on non-planar, complex

substrates. These results open prospects for the interface engineering of membranes or electrolyzers, where precise coatings of tubular surfaces are needed.

Keywords

Inorganic membrane, Spatial Atomic Layer Deposition, 3D printing, tubular substrates, interface engineering

1. Introduction

The development of highly efficient membranes has become of central interest for the energy sector and the chemical industry, as the efficient separation of species represents a valuable strategy to reduce cost, energy, and environmental impact of many processes[1,>] or to reduce the impact of human activities by eliminaton of pollutants in wastewater and contaminated air. One example of current membrane energy application is the membrane-assisted separation of hydrogen for its use as energy carrier [3–8], which is expected to be fundamental for the forthcoming shift to carbon-neutral societies. Coupling membranes to chemical industry is a key strategy for intensification of processes such as Fischer-Tropsch, aromatization, de/hydrogenation, reforming [9–12] and membrane reactors in general [13].

The separation processes are achieved by enabling species/molecules to pass through the membrane as a result of a driving force. Most transport processes take place because of a difference in chemical potential (pressure and concentration contribute to the chemical potential). Depending on their architecture, membranes achieve fluid separation through either i) solution-diffusion, if a dense film of the appropriate material is used, or ii) molecular sieving, for appropriate porous films. In particular, tubular-shaped membranes are appealing to industry since they offer strong adaptability, easier sealing, high-pressure resistance and higher modularity than their planar counterparts. Such membranes can be prepared by dip-coating or spray-coating of tubular supports by sol-gel routes (plus spin coating or screen printing for planar membranes), but the precise control of chemical and physical properties of both dense and porous membranes (i.e., thickness, surface composition, pore size, etc.) is still a key challenge for membrane producers [1,>]. Thus, thin films are highly attractive for the coating of dense membranes, as it decreases the amount of material required (especially for expensive or scarce elements) while improving the permeability. In addition, thin film techniques can enable a precise control of the pore size for porous membranes.

Among thin film deposition techniques enabling tubular coatings, physical vapor deposition (PVD) techniques have a low energy-efficiency and spinning systems are required (including heating elements) which increase the complexity and/or cost. Electrodeposition and solvothermal approaches can be used for the deposition of metals and simpler oxides with lower use of consumables and at lower cost. However, these approaches require more steps, yield thicker layers and there are also several concerns from the health, safety and environmental points of view [1>]. As recently reviewed, chemical vapor deposition (CVD) techniques such as atomic layer deposition (ALD) are extremely valuable for membrane science and have been tested for many applications, including gas separation and water filtration, biosensing and catalysis [15–17]. ALD is based on the sequential use of surface-limited, self-terminating chemical reactions that take place in a cycle-wise fashion, thus allowing to prepare conformal and high quality films at the nanoscale on complex substrates and at low temperatures [18–20]. ALD has traditionally been a vacuum-based technique requiring the use of relatively costly reactors and pumping systems. Spatial atomic layer deposition (SALD) is a branch of conventional ALD, in which the precursors are continuously injected in different locations of the reactor, being separated by a flow of inert gas. This technique is able to reach faster growth rates than conventional ALD and can be performed at atmospheric pressure and in the open air (i.e. without deposition chamber) [21,22]. This does not compromise the deposition of high quality materials, even on high-aspect -ratio substrates, with precise thickness control, high uniformity and excellent conformality [23–25].

SALD can indeed be implemented in different ways [2>]. This work is based on the close-proximity manifold approach [27,28], where the reactants are distributed along adjacent channels and separated by inert gas and exhausts channels [29]. The close proximity of the substrate to the head then ensures the efficient separation of the reactants. The movement of the substrate exposes the surface to the different reactants, therefore reproducing the layer-by-layer growth of conventional ALD. This SALD approach is particularly versatile since it can be easily tuned by simply modifying the manifold injector. For instance, we have shown that 3D printing can be used to customize close-proximity SALD manifolds in different materials, opening up a large span of possibilities [30,31].

However, SALD has been only used to coat planar substrates such as wafers, glasses, or flat polymeric substrates so far. Porous materials or high-aspect-ratio features have also been coated, but the macroscopic nature of these samples is a flat substrate. A notable exception has been reported van Ommen's group where the coating of nanoparticles was enabled by implementing a SALD system in a fluidized reactor [32]. In this work, we take advantage of 3D printing to design a gas manifold specifically tailored for tubular supports. To demonstrate the feasibility to perform SALD on such tubular surfaces, ZnO layers have been deposited on Cu foils wrapped around tubular supports and on Al_2O_3 tubular porous membrane substrates. This work is a new versatile way of printing functional devices to extend the current potential of SALD[33–35] to membrane applications, opening a new avenue in the field for coating complex substrates with functional materials.

2. Materials and Methods

2.1. SALD of ZnO on tubular supports

The gas manifold was elaborated through computer-aided design (CAD) in Solid Edge and 3D printed by stereolithography (FORM2, Formlabs) with Clear V4 (Formlabs). Supports and resin leftovers were carefully removed and the 3D-piece was cleaned with isopropanol (<99.8% purity, Honeywell) and cautiously dried prior to SALD deposition. Simulations of the gas pressure distribution among the prechambers and gas outlet channels within the SALD gas manifolds were performed in COMSOL Multiphysics software using the CFD module.

ZnO was deposited at room temperature using a custom-made atmospheric pressure SALD system [3]>. Two substrates were considered : i) Cu foils (3M) wrapped around 3D printed polymer tubes of 1 cm diameter, and ii) commercial Al_2O_3 porous tubular membranes (50 nm pore size diameter, Atech Innovations GmbH) of 1 cm outer diameter. Diethylzinc (DEZ, $Zn(C_2H_5)_2$, Sigma Aldrich) and water

(H_2O) were used as metal precursor and coreactant respectively. Nitrogen (99.995%, AirLiquide) was used both as a carrying gas in precursor lines and as barrier gas in dedicated lines separating DEZ and water flows. The precursors were carried from the bubblers to the gas manifold by flowing 15 and 90 sccm of nitrogen through the DEZ and water bubblers, and were subsequently diluted with 135 and 210 sccm of additional nitrogen, respectively. The total nitrogen flowrate used as barrier gas was 600 sccm.

2.2. Characterization Techniques

The morphology of the deposited ZnO thin films was investigated by field-emission scanning electron microscopy (FESEM) using a Zeiss Gemini 300 field-emission-gun scanning electron microscope. FESEM energy-dispersive X-ray spectroscopy (EDS) spectra were recorded using a Bruker X-ray detector incorporated in the Zeiss Gemini 300 field-emission-gun scanning electron microscope operating at 15 kV. X-ray diffraction (XRD) patterns were collected with a Rigaku SmartLab diffractometer equipped with a rotating Cu anode operating at 9 kW (45 kV and 200 mA) from which the Cu $K\alpha_1$ radiation was used. The θ-2θ scans were performed in the standard Bragg−Brentano configuration with a step of 0.1° and a speed of 0.3° s^{-1} using parallel beams (divergence less than 0.05°). The ZnO and α-Al_2O_3 diffraction peaks were indexed according to the ICDD 00-036-145 and 00-046-1212 files, respectively.

3. Results and Discussion

3.1. Design and fabrication of the tubular gas manifold

The possibility to 3D print gas manifolds enable the integration of gas distribution and separation circuits into the body as shown in our group previously [30,3]>. In this work, we take further advantage of these capabilities to design a gas manifold for deposition on tubular substrates based in the same close-proximity technology. More specifically, a cylindric gas manifold dedicated to the SALD of tubular surfaces was fabricated through CAD and 3D printing, as illustrated in Fig. 1. The gas manifold contains four external connections, as revealed by Fig. 1a, being the inlets for metal precursor, coreactant, inert gas, and the exhaust outlet. In this configuration, the tubular substrate is introduced in the central cyclindrical hole of the gas manifold and moves back and forth during deposition to ensure the exposition of its surface to the different gases. The hole diameter can be easily adjusted to the substrate diameter in order to have a controlled gap in the range of 50-200 µm between the substrate surface and the gas outlets. Furthermore, both inlet and outlet channels connect to individual concentric prechambers located within the the bulk of the gas manifold as detailed in the cross-section view shown in Fig. 1b. These prechambers have a concentric outlet channel facing the substrate to ensure the exposure of the substrate to the gases or to extract them.

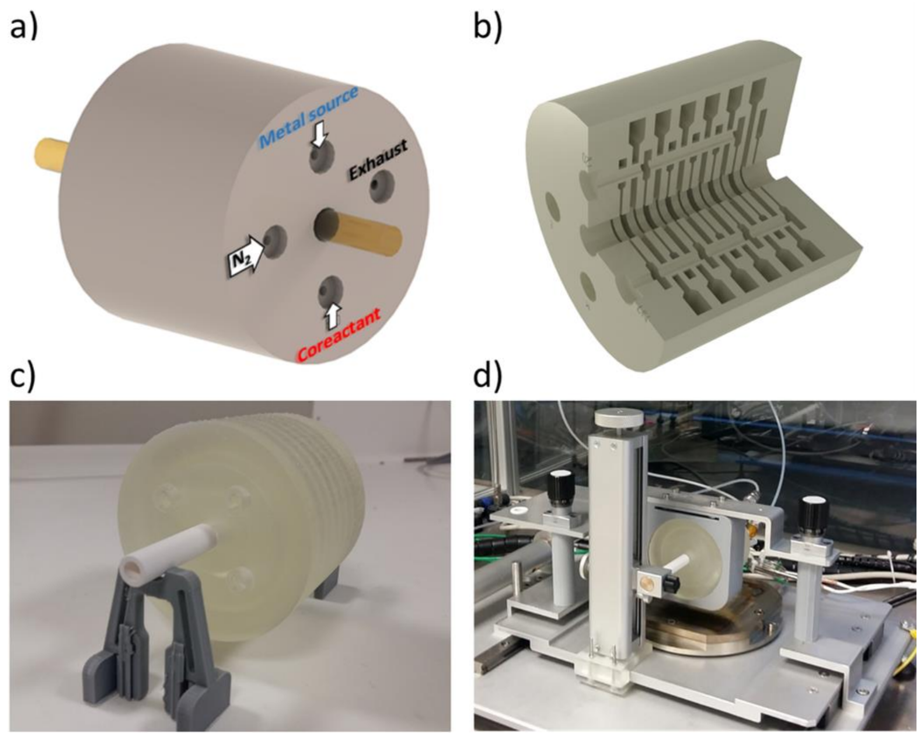

Fig. 1. (a) Scheme of the cylindrical SALD manifold designed to coat tubular substrates, (b) detailed cross-section view of the design, (c) printed version of the gas manifold, and (d) integration into the custom-made SALD system.

The concentric prechambers are required to ensure a good homogeneization of the gas pressure and its proper distribution through the outlet channel. An inappropriate design would lead to inhomogeneous deposition with unexposed areas on the tubular substrate [35]. Prior to the design, COMSOL Multiphysics simulations using the CFD module were performed to find adequate ratios between the prechamber and the channel outlet volumes offering optimal gas pressure distributions, whose results are summarized in Fig. 2. The study was performed on an individual 3D channel of a standard SALD gas manifold [39] for the sake of time and hardware requirements. There are two inlets in each side of the prechamber, and one outlet at the bottom of the channel where the substrate is located. As stated before, the flow and pressure through the prechamber and channel oulet are evaluated to check the size of prechamber yielding a good homogeneity of the gas, i.e. a constant flow front reaching the substrate surface. Otherwise, prefential pathways, extended regions with different gas speeds, or dead zones where no gas flow occur can be generated, leading to an innacurate gas distribution and a lack of homogeneity in the deposition. To do so, the channel outlet volume was kept constant (with channel dimensions fixed at 50 × 15 × 0.5 mm^3) and the radius of the prechamber was varied from 1 to 2 mm. Moreover, a constant flowrate of 100 mL/min was applied to both prechamber inlets. The results reveal that a small prechamber volume (i.e. with a radius of 1 mm, Fig. 2a) should be avoided as it produces very inhomogeneous gas flow distribution along the outlet channel. The homogeneity of the gas is drastically improved when increasing the prechamber volume (i.e. when increasing its radius above 1 mm, Fig. 2b-d), a minimum radii between 1.4 and 2 mm is required to ensure good homogeneization (Fig. 2c,d). Therefore, as a general rule, a prechamber/channel outlet volume ratio of at least 0.8 should be respected for the design of the cylindrical SALD manifold.

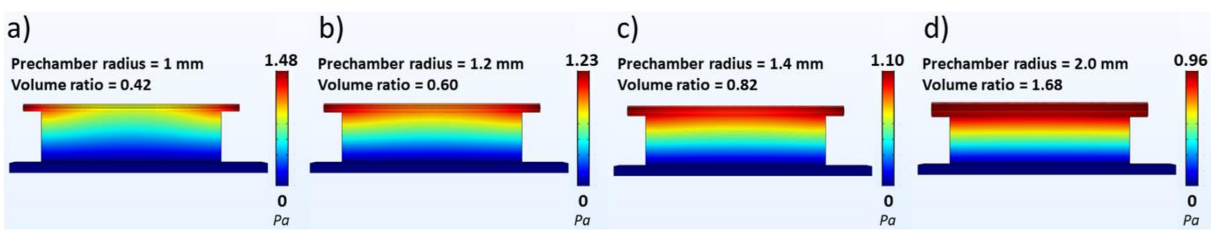

Fig. 2. CFD calculations made with COMSOL Multiphysics, where the fluid distribution is assessed along an outlet channel for varying prechamber radii of (a) 1 mm, (b) 1.2 mm, (c) 1.4 mm, and (d) 2.0 mm. The corresponding prechamber/chanel outlet volume ratios are also indicated.

The concentric nature of the gas manifold also adds some complexity to the 3D printing process. Indeed, to guarantee its feasibility, temporary supports must be printed in the central hole where the substrate is to be placed. However, the smoothness of this internal surface is capital for the deposition process ensuring an even distribution of the flow. The supports were thus removed carefully and the internal cylindrical surface was polished with fine polishing paper (1200) to smooth the surface. Additionnally, a thorough cleaning of the inner channels with isopropanol followed by a drying process must be done to avoid any loss of shape or blockage of the outer channels due to resin or liquid accumulation. A Dino-Lite RK-10 holder with integrated z-axis controller is used as a sample holder to accurately control the height of the tubular sample, providing precise alignment with the gas manifold. The sample holder is secured by a 3D printed home-made piece to the SALD moving plate, tightening the tubular sample at its position at the center of the gas manifold and ensuring an appropriate gap with gas outlets (Fig. 1d).

3.2. SALD of ZnO on tubular substrates

A first validation of the gas manifold design and integration into the SALD system was performed using 3D printed tubes of 1 cm diameter wrapped with Cu foils as tubular substrates. Cu foils permit the visual identification of the deposition through their change of contrast, and they can be easily unwrapped from the 3D printed tubes for later characterization in SEM. ZnO was choosen because it is a school-case ALD material and because the group has extensive expertise in its deposition [36,3>]. Additionally, amorphous ZnO can be grown at room temperature facilitating the operational validation of the gas manifold. Standard SALD conditions previously reported for ZnO deposition ([36,39] on planar substrates) were tested successfully as depicted in Fig. 3a. The deposition distance (i.e. the amplitude of the substrate displacement) was varied and the related changes of contrast observed confirm that the deposition is taking place in the desired region, which can thus be typically controlled in the range of a few centimeters. Moreover, FESEM observations of the Cu foils (Fig. 3b,c) confirm the growth of a ZnO thin film in the region exposed to precursors, while no ZnO is observed in the pristine region. The ZnO layer covers the whole surface exposed, with no apparent change between regions. The deposition of ZnO is further confirmed by FESEM-EDS analyses (Fig. 3d), where a significant signal associated to the $Zn_{K\alpha}$ energy transition is observed at around 8.6 keV in the region exposed to precursors, while this signal is absent on the pristine Cu foil.

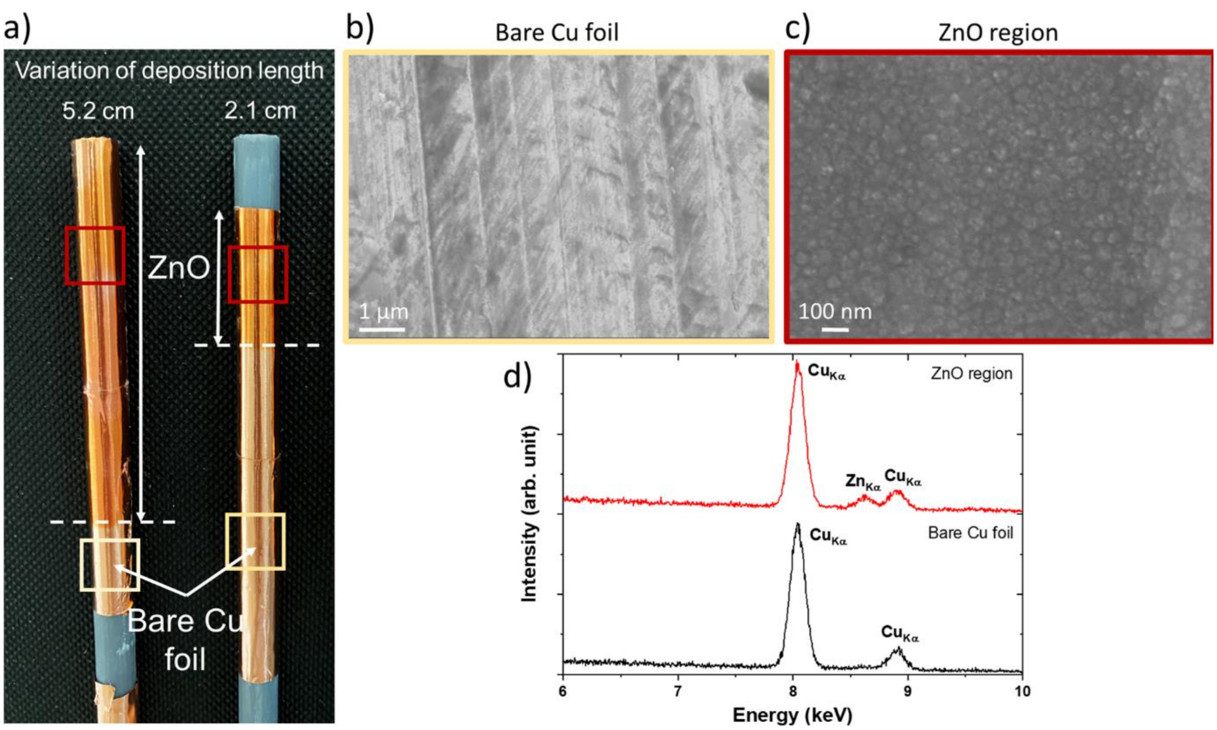

Fig. 3. (a) Cu foils with ZnO depositions along variable lengths. Top-view FESEM images of (b) a bare Cu foil and of (c) a Cu foil with ZnO deposition. (d) Corresponding FESEM-EDS spectra.

In a second step, we aimed to confirm the potential of this new approach for the surface engineering of membrane supports by using the 3D printed gas manifold to perform SALD on porous α-Al_2O_3 tubular ceramic supports (50 nm pore size), such as the one presented in Fig. 4a. The equivalent to 1000 conventional ALD cycles were used for deposition of ZnO. FESEM observations revealed the deposition of a ZnO thin layer with an estimated thickness of 400 nm, corresponding to a growth rate of 4 Å/cycle (Fig. 4b,c). It can be noted that the growth rate is higher than what is typically expected for an ALD process, implying a major CVD contribution during the ZnO deposition. Indeed, the possibility to grow both in CVD and ALD mode is one of the advantages offered by close-proximity SALD based on manifold heads. Deposition in SCVD mode has been used in the past and, for surfaces with no complex or high-aspect-ratio features, homogeneous films can be obtained with GPC values larger than for the equivalen ALD process. The optimization of the tubular head presented here is possible for the cases when ALD conditions are required. These optimizations will involve the adjustment of parameters such as the flow rates, the gap between the gas manifold and the sample surface, the channel width and separation, and the sample movement speed. A strong associated signal of the $Zn_{L\alpha}$ energy transition at around 1.0 eV is further measured from FESEM-EDS characterizations in areas exposed to the chemical precurors (otherwise absent on the bare membrane), confirming the ZnO chemical nature of the thin layer (Fig. 4d). Moreover, different membrane pieces were characterized by XRD to gain more insights on their structural properties. To ensure good crystallization of the ZnO thin film, the samples were annealed at 500 °C during 1 h. The obtained XRD patterns in the deposited region, shown in Fig. 4e, clearly reveal the presence of several diffraction peaks associated to wurtzite ZnO, while only diffraction peaks associated to α-Al_2O_3 are present on the bare membrane. These results demonstrate the great potential of SALD for the deposition of high quality thin films on complex substrates such as tubular membrane supports. Additionnally, the repeatability of the depositions and reuse of the gas manifold can be typically achieved through a proper alignment of the sample using the level adjuster described previously and a thorough gas manifold maintenance (cleaning with 5% nitric acid solution, rinsing with isopropanol and drying), respectively.

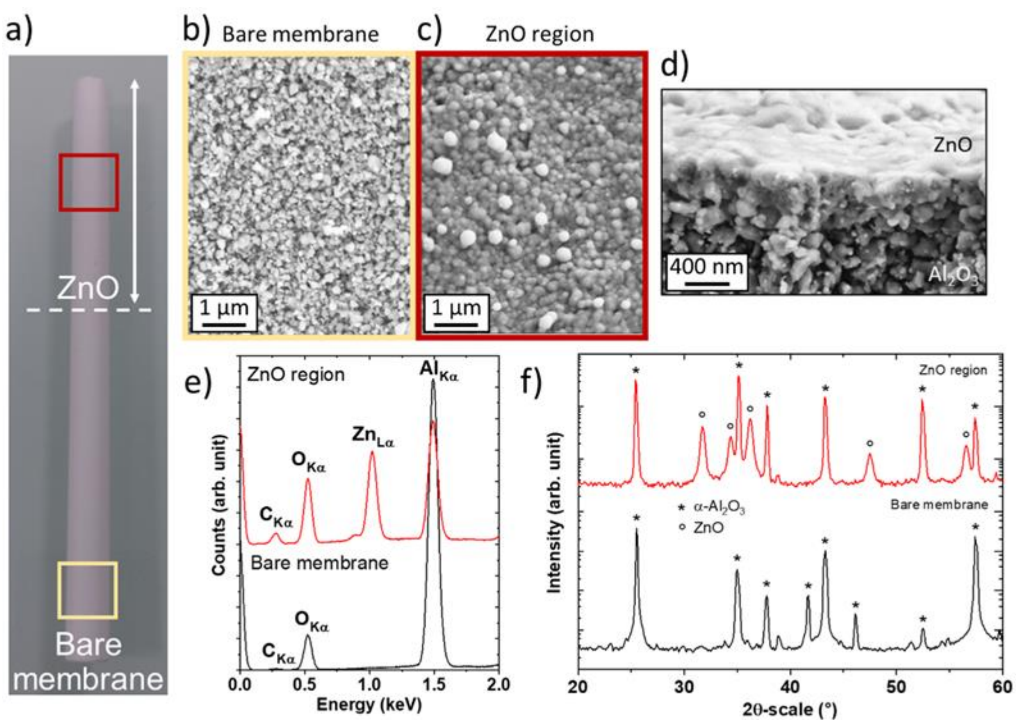

Fig. 4. (a) Tubular membrane support after ZnO deposition. (b,c) Top-view FESEM images of the membrane (b) without and (c) with ZnO deposition. (d) High-magnification cross-section view of the ZnO thin film. (e) Corresponding FESEM-EDS spectra, and (f) XRD patterns of membrane pieces without and with ZnO deposition after annealing at 500 °C.

3.3 Perspectives

The present work shows a proof of concept reporting the coating of tubular membranes by an an open-air technique (SALD) which is attractive for interface enginering because of both conformal coating and excellent thickness control. For example, some ALD-prepared materials such as palladium or metal-organic frameworks (MOFs) are particularly relevant for the fabrication of separation membranes [40,41]. It is worth noting that thin films such as ZnO can be subsequently converted to a MOF by hydrothermal techniques. Heating elements can also be easily incorporated to the system to enable the deposition of materials not available at room temperature.

Capability to deposit dense thin layers over porous tubular supports enables the use of SALD for the coating of dense membranes as well as other electrochemical devices such as fuel cells/electrolyzers or electrochemical membrane reactors with tailored electrodes [42–51], where the gas separation occurs by adsorption and diffusion through the thin layer. Different ionic and protonic materials comprising more complex oxides or metals have already been deposited by ALD [52–60], and their addition to the SALD palette for both planar and tubular depositions would be appealing for various industrial applications. Moreover, the gas manifold design could be adapted for the coating of other types of non-planar substrates, which could be used in various applications such as free-form electronics [61] or for curved lenses and mirrors fabrication [62,63].

SALD gas manifolds can be also modular (coupling several manifolds in series) enlarging the deposition area. This can be also used to tailor deposition i.e. different modules with alternating materials can be used to have multimaterial and multifunctional devices.

4. Conclusions

In this work, we successfully performed thin film deposition on tubular substrates using the atmospheric pressure SALD technique in the open-air close-proximity approach. Using computational fluid dynamics calculations, an innovative SALD gas manifold has been designed and fabricated thanks to the versatility offered by 3D printing. The custom gas manfiold has been designed to deliver a concentric homogeneous precursor gas outflow covering the whole surface of tubular substrates. The relations between the different volumes within the gas manifols has been evaluated by means of COMSOL Multiphysics. Using DEZ and water as precursors, the design of the gas manifold has been validated by depositing ZnO onto Cu foils and porous alumina tubular supports. The successful depositions show the high potential of SALD for the engineering of membrane interfaces. Further optimization will result in heads in which the ALD and CVD mode can be precisely controlled by adjusting the different flows. These results open the door to the high-throughput fabrication of both dense and porous tubular membranes of various materials by SALD. This approach can be further adapted to the preparation of other nanomaterials as well as to other substrate geometries, widening the field of applications of SALD on complex surfaces.

AUTHOR INFORMATION

Corresponding Author

* Corresponding author 1. *E-mail address*: fitolrei@itq.upv.es (D. Fidel Toldrá Reig)

** Corresponding author 2. *E-mail address*: david.munoz-rojas@grenoble-inp.fr (D. Muñoz-Rojas)

Present Addresses

† Current Address: Instituto de Tecnología Química (CSIC-UPV), Universitat Politècnica de València, Camino de vera s/n, 46022, Valencia, Spain

Author Contributions

The manuscript was written through contributions of all authors. All authors have given approval to the final version of the manuscript.

Funding Sources

This work was supported by the French Research National Agency through the project ALD4MEM (ANR ANR-20-CE09-0008).

Acknowledgments

The authors thankthe French Reseach National Agency for funding (ANR ANR-20-CE09-0008) and Hervé Roussel from LMGP for the XRD characterizations.

References

(1) Zydney, A. L. *Membrane Handbook, Winston Ho, W. S.; Sirkar, K.K.; Reinhold, V.N.; Eds.;* John Wiley & Sons, Ltd*, New York, 1992,* AIChE J. 41 **1995**, 2343–2344.. DOI: 10.1002/AIC.690411024.

(2) *Comprehensive Membrane Science and Engineering (Second Edition)* Drioli, E.; Giorno, L., Fontananova, E., Eds. ; Elsevier: London, **2017**.

(3) Ivanova, M. E.; Escolástico, S.; Balaguer, M.; Palisaitis, J.; Sohn, Y. J.; Meulenberg, W. A.; Guillon, O.; Mayer, J.; Serra, J. M. Hydrogen Separation through Tailored Dual Phase Membranes with Nominal Composition BaCe0.8Eu0.2O 3- δ :Ce0.8Y0.2O2-δ at Intermediate Temperatures. *Nat. Publ. Gr.* **2016,** 6, 34773. DOI: 10.1038/srep34773.

(4) Iwahara, H.; Asakura, Y.; Katahira, K.; Tanaka, M. Prospect of Hydrogen Technology Using Proton-Conducting Ceramics. In *Solid State Ionics* **2004**, 168, 299–310. DOI: 10.1016/j.ssi.2003.03.001.

(5) Gallucci, F.; Medrano, J. A.; Fernandez, E.; Melendez, J.; Van Sint Annaland, M.; Pacheco-Tanaka, D. A. Advances on High Temperature Pd-Based Membranes and Membrane Reactors for Hydrogen Purifcation and Production. *Journal of Membrane Science and Research*. **2017**, 3, 142–156. DOI: 10.22079/jmsr.2017.23644.

(6) Jeong, S. W.; Yamaguchi, T.; Okamoto, M.; Zhu, C.; Habazaki, H.; Nagayama, M.; Aoki, Y. Proton Pumping Boosts Energy Conversion in Hydrogen-Permeable Metal-Supported Protonic Fuel Cells. *ACS Appl. Energy Mater.* **2020**, *3* (1), 1222–1234. DOI: 10.1021/acsaem.9b02287.

(7) Meng, T.; Young, K.; Beglau, D.; Yan, S.; Zeng, P.; Cheng, M. M.-C. Hydrogenated Amorphous Silicon Thin Film Anode for Proton Conducting Batteries. *J. Power Sources* **2016**, *302*, 31–38. DOI: 10.1016/J.JPOWSOUR.2015.10.045.

(8) Itoh, N.; Xu, W. .; Hara, S.; Sakaki, K. Electrochemical Coupling of Benzene Hydrogenation and Water Electrolysis. *Catal. Today* **2000**, *56* (1–3), 307–314. DOI: 10.1016/S0920-5861(99)00288-6.

(9) Serra, J. M. Electrifying Chemistry with Protonic Cells. *Nat. Energy* **2019**, *4* (3), 178–179. DOI: 10.1038/s41560-019-0353-y.

(10) Escorihuela, S.; Toldra-Reig, F.; Escolástico, S.; Murciano, R.; Martínez, A.; Serra, J. M. Copper Surface-Alloying of H2-Permeable Pd-Based Membrane for Integration in Fischer–Tropsch Synthesis Reactors. *J. Memb. Sci.* **2021**, *619, 118516*. DOI: 10.1016/j.memsci.2020.118516.

(11) Solís, C.; Toldra-Reig, F.; Balaguer, M.; Somacescu, S.; Garcia-Fayos, J.; Palafox, E.; Serra, J. M. Mixed Ionic–Electronic Conduction in NiFe2O4–Ce0.8Gd0.2O2− δ Nanocomposite Thin Films for Oxygen Separation. *ChemSusChem* **2018**, 11, 2818 –2827. DOI: 10.1002/cssc.201800420.

(12) Malerød-Fjeld, H.; Clark, D.; Yuste-Tirados, I.; Zanón, R.; Catalán-Martinez, D.; Beeaff, D.; Morejudo, S. H.; Vestre, P. K.; Norby, T.; Haugsrud, R.; Serra, J. M.; Kjølseth, C. Thermo-Electrochemical Production of Compressed Hydrogen from Methane with near-Zero Energy Loss. *Nat. Energy* **2017**, *2* (12), 923–931. DOI: 10.1038/s41560-017-0029-4.

(13) Arratibel Plazaola, A.; Pacheco Tanaka, D. A.; Van Sint Annaland, M.; Gallucci, F. Recent Advances in Pd-Based Membranes for Membrane Reactors. *Molecules* **2017**, 22, 51 DOI: 10.3390/molecules22010051.

(14) Merlo, A.; Léonard, G. Magnetron Sputtering vs. Electrodeposition for Hard Chrome Coatings: A

Comparison of Environmental and Economic Performances **2021**, *14* (14), 3823. DOI: 10.3390/MA14143823/S1.

(15) Weber, M.; Julbe, A.; Kim, S. S.; Bechelany, M. Atomic Layer Deposition (ALD) on Inorganic or Polymeric Membranes. *J. Appl. Phys.* **2019**, *126* (4), 041101. DOI: 10.1063/1.5103212.

(16) Weber, M.; Julbe, A.; Ayral, A.; Miele, P.; Bechelany, M. Atomic Layer Deposition for Membranes: Basics, Challenges, and Opportunities. *Chem. Mater.* **2018**, *30* (21), 7368–7390. DOI: 10.1021/acs.chemmater.8b02687.

(17) Yang, H. C.; Waldman, R. Z.; Chen, Z.; Darling, S. B. Atomic Layer Deposition for Membrane Interface Engineering. *Nanoscale*. Royal Society of Chemistry November 28, 2018, pp 20505–20513. DOI: 10.1039/c8nr08114j.

(18) George, S. M. Atomic Layer Deposition: An Overview. *Chem. Rev.* **2010**, *110* (1), 111–131. DOI: 10.1021/cr900056b.

(19) Johnson, R. W.; Hultqvist, A.; Bent, S. F. A Brief Review of Atomic Layer Deposition: From Fundamentals to Applications. *Mater. Today* **2014**, *17* (5), 236–246. DOI: 10.1016/j.mattod.2014.04.026.

(20) Leskelä, M.; Ritala, M. Atomic Layer Deposition (ALD): From Precursors to Thin Film Structures. *Thin Solid Films* **2002**, *409* (1), 138–146. DOI: 10.1016/S0040-6090(02)00117-7.

(21) Muñoz-Rojas, D.; Macmanus-Driscoll, J. Spatial Atmospheric Atomic Layer Deposition: A New Laboratory and Industrial Tool for Low-Cost Photovoltaics. *Materials Horizons* **2014**, 1, 314–320. DOI: 10.1039/c3mh00136a.

(22) Muñoz-Rojas, D.; Maindron, T.; Esteve, A.; Piallat, F.; Kools, J. C. S.; Decams, J.-M. Speeding up the Unique Assets of Atomic Layer Deposition. *Mater. Today Chem.* **2019**, *12*, 96–120. DOI: 10.1016/J.MTCHEM.2018.11.013.

(23) Musselman, K. P.; Muñoz-Rojas, D.; Hoye, R. L. Z.; Sun, H.; Sahonta, S. L.; Croft, E.; Böhm, M. L.; Ducati, C.; MacManus-Driscoll, J. L. Rapid Open-Air Deposition of Uniform, Nanoscale, Functional Coatings on Nanorod Arrays. *Nanoscale Horizons* **2017**, *2* (2), 110–117. DOI: 10.1039/C6NH00197A.

(24) Nguyen, V. S.; Sekkat, A.; Bellet, D.; Chichignoud, G.; Kaminski-Cachopo, A.; Muñoz-Rojas, D.; Favre, W. Open-Air, Low-Temperature Deposition of Phase Pure Cu2O Thin Films as Efficient Hole-Transporting Layers for Silicon Heterojunction Solar Cells. *J. Mater. Chem. A* **2021**, *9* (29), 15968–15974. DOI: 10.1039/D1TA02931B.

(25) Nguyen, V. H.; Resende, J.; Papanastasiou, D. T.; Fontanals, N.; Jiménez, C.; Muñoz-Rojas, D.; Bellet, D. Low-Cost Fabrication of Flexible Transparent Electrodes Based on Al Doped ZnO and Silver Nanowire Nanocomposites: Impact of the Network Density †. *Nanoscale* **2019**, *11*, 12097. DOI: 10.1039/c9nr02664a.

(26) Muñoz-Rojas, D.; Huong Nguyen, V.; Masse de la Huerta, C.; Jiménez, C.; Bellet, D. Spatial Atomic Layer Deposition. In *Chemical Vapor Deposition for Nanotechnology*; IntechOpen, **2019**. DOI: 10.5772/intechopen.82439.

(27) Levy, D. H.; Freeman, D.; Nelson, S. F.; Cowdery-Corvan, P. J.; Irving, L. M. Stable ZnO Thin Film Transistors by Fast Open Air Atomic Layer Deposition. *Appl. Phys. Lett.* **2008**, *92* (19). DOI: 10.1063/1.2924768.

(28) Muñoz-Rojas, D.; Sun, H.; Iza, D. C.; Weickert, J.; Chen, L.; Wang, H.; Schmidt-Mende, L.; MacManus-Driscoll, J. L. High-Speed Atmospheric Atomic Layer Deposition of Ultra Thin

Amorphous TiO2 Blocking Layers at 100 °C for Inverted Bulk Heterojunction Solar Cells. *Prog. Photovoltaics Res. Appl.* **2013**, *21* (4), 393–400. DOI: 10.1002/PIP.2380.

(29) Levy David H. Process for Atomic Layer Deposition. US-7413982-B2, **2008**.

(30) de la Huerta, C. A. M.; Nguyen, V. H.; Sekkat, A.; Crivello, C.; Toldra-Reig, F.; Veiga, P. B.; Quessada, S.; Jimenez, C.; Muñoz-Rojas, D. Gas-Phase 3D Printing of Functional Materials. *Adv. Mater. Technol.* **2020**, 5, 2000657. DOI: 10.1002/admt.202000657.

(31) Muñoz-Rojas, D.; Weber, M.; Va L L É E, C.; Crivello, C.; Sekkat, A.; Toldra-Reig, F.; Bechelany, M. Nanometric 3D Printing of Functional Materials by Atomic Layer Deposition. *Adv. Addit. Manuf.; IntechOpen,* **2022**. DOI: 10.5772/INTECHOPEN.101859.

(32) Ommen, J. R. van; Kooijman, D.; Niet, M. de; Talebi, M.; Goulas, A. Continuous Production of Nanostructured Particles Using Spatial Atomic Layer Deposition. *J. Vac. Sci. Technol. A Vacuum, Surfaces, Film.* **2015**, *33* (2), 021513. DOI: 10.1116/1.4905725.

(33) Li, J.; Pumera, M. 3D Printing of Functional Microrobots. *Chem. Soc. Rev.* **2021**, *50* (4), 2794–2838. DOI: 10.1039/D0CS01062F.

(34) Browne, M. P.; Plutnar, J.; Pourrahimi, A. M.; Sofer, Z.; Pumera, M. Atomic Layer Deposition as a General Method Turns Any 3D-Printed Electrode into a Desired Catalyst: Case Study in Photoelectrochemisty. *Adv. Energy Mater.* **2019**, *9* (26), 1900994.

(35) Ng, S.; Zazpe, R.; Rodriguez-Pereira, J.; Michalička, J.; Macak, J. M.; Pumera, M. Atomic Layer Deposition of Photoelectrocatalytic Material on 3D-Printed Nanocarbon Structures. *J. Mater. Chem. A* **2021**, *9* (18), 11405–11414.

(36) Nguyen, V. H.; Resende, J.; Jiménez, C.; Deschanvres, J.-L.; Carroy, P.; Muñoz, D.; Bellet, D.; Muñoz-Rojas, D. Deposition of ZnO Based Thin Films by Atmospheric Pressure Spatial Atomic Layer Deposition for Application in Solar Cells. *J. Renew. Sustain. Energy* **2017**, *9* (2), 021203. DOI: 10.1063/1.4979822.

(37) Nguyen, V. H.; Sekkat, A.; Masse De La Huerta, C. A.; Zoubian, F.; Crivello, C.; Rubio-Zuazo, J.; Rubio-Zuazo, J.; Jaffal, M.; Bonvalot, M.; Vallée, C.; Aubry, O.; Rabat, H.; Hong, D.; Muñoz-Rojas, D. Atmospheric Plasma-Enhanced Spatial Chemical Vapor Deposition of SiO2Using Trivinylmethoxysilane and Oxygen Plasma. *Chem. Mater.* **2020**, *32* (12), 5153–5161. DOI: 10.1021/ACS.CHEMMATER.0C01148.

(38) de la Huerta, C. M.; Nguyen, V. H.; Dedulle, J. M.; Bellet, D.; Jiménez, C.; Muñoz-Rojas, D. Influence of the Geometric Parameters on the Deposition Mode in Spatial Atomic Layer Deposition: A Novel Approach to Area-Selective Deposition. *Coatings* **2018**, *9* (1), 5. DOI: 10.3390/COATINGS9010005.

(39) Nguyen, V. H.; Sekkat, A.; Jiménez, C.; Muñoz, D.; Bellet, D.; Muñoz-Rojas, D. Impact of Precursor Exposure on Process Efficiency and Film Properties in Spatial Atomic Layer Deposition. *Chem. Eng. J.* **2021**, *403*, 126234. DOI: 10.1016/j.cej.2020.126234.

(40) Weber, M.; Drobek, M.; Rebière, B.; Charmette, C.; Cartier, J.; Julbe, A.; Bechelany, M. Hydrogen Selective Palladium-Alumina Composite Membranes Prepared by Atomic Layer Deposition. *J. Memb. Sci.* **2020**, *596*, 117701. DOI: 10.1016/j.memsci.2019.117701.

(41) Weber, M.; Bechelany, M. Combining Nanoparticles Grown by ALD and MOFs for Gas Separation and Catalysis Applications. *Pure Appl. Chem.* **2020**, *92* (2), 213–222. DOI: 10.1515/PAC-2019-0109.

(42) Vøllestad, E.; Strandbakke, R.; Tarach, M.; Catalán-Martínez, D.; Fontaine, M. L.; Beeaff, D.;

Clark, D. R.; Serra, J. M.; Norby, T. Mixed Proton and Electron Conducting Double Perovskite Anodes for Stable and Efficient Tubular Proton Ceramic Electrolysers. *Nat. Mater.* **2019**, *18* (7), 752–759. DOI: 10.1038/s41563-019-0388-2.

(43) Morejudo, S. H.; Zanón, R.; Escolástico, S.; Yuste-Tirados, I.; Malerød-Fjeld, H.; Vestre, P. K.; Coors, W. G.; Martínez, A.; Norby, T.; Serra, J. M.; Kjølseth, C. Direct Conversion of Methane to Aromatics in a Catalytic Co-Ionic Membrane Reactor. *Science (80-.).* **2016**, *353* (6299), 563–566. DOI: 10.1126/SCIENCE.AAG0274.

(44) Tan, X. Y.; Yin, W. N.; Meng, B.; Meng, X. X.; Yang, N. T.; Ma, Z. F. Preparation of Electrolyte Membranes for Micro Tubular Solid Oxide Fuel Cells. *Sci. China Ser. B Chem. 2008 519* **2008**, *51* (9), 808–812. DOI: 10.1007/S11426-008-0068-6.

(45) Zhu, L.; O'Hayre, R.; Sullivan, N. P. High Performance Tubular Protonic Ceramic Fuel Cells via Highly-Scalable Extrusion Process. *Int. J. Hydrogen Energy* **2021**, *46* (54), 27784–27792. DOI: 10.1016/J.IJHYDENE.2021.06.018.

(46) Agbede, O. O.; Hellgardt, K.; Kelsall, G. H. Electrical Conductivities and Microstructures of LSM, LSM-YSZ and LSM-YSZ/LSM Cathodes Fabricated on YSZ Electrolyte Hollow Fibres by Dip-Coating. *Mater. Today Chem.* **2020**, *16*, 100252. DOI: 10.1016/J.MTCHEM.2020.100252.

(47) Kleiminger, L.; Li, T.; Li, K.; Kelsall, G. H. Syngas (CO-H2) Production Using High Temperature Micro-Tubular Solid Oxide Electrolysers. *Electrochim. Acta* **2015**, *179*, 565–577. DOI: 10.1016/J.ELECTACTA.2015.07.062.

(48) Morales, M.; Laguna-Bercero, M. A. Microtubular Solid Oxide Fuel Cells Fabricated by Gel-Casting: The Role of Supporting Microstructure on the Mechanical Properties. *RSC Adv.* **2017**, *7* (29), 17620–17628. DOI: 10.1039/C7RA01259D.

(49) Kherad, R.; Dodangei, S.; Moussavi, S. H.; Ghatee, M. Characterization of Anode Supported Micro-Tubular Solid Oxide Fuel Cells Prepared by Successive Non-Aqueous Electrophoretic Deposition. *J. Electroceramics* **2021**, *1*, 1–7. DOI: 10.1007/S10832-021-00272-5.

(50) Li, Y.; Chen, L.; Zhang, L.; Xia, C. Millimeter Tubular Solid Oxide Electrolysis Cells with Modified Asymmetric Hydrogen Electrode. *Int. J. Hydrogen Energy* **2016**, *41* (10), 5209–5214. DOI: 10.1016/J.IJHYDENE.2016.01.103.

(51) Tan, Z.; Ishihara, T. Effect of Ni-Based Cathodic Layer on Intermediate Temperature Tubular Electrolysis Cell Using LaGaO3-Based Electrolyte Thin Film. *JPhys Energy* **2020**, *2* (2), 024004. DOI: 10.1088/2515-7655/ab6f4b.

(52) Gong, T.; Huang, Y.; Qin, L.; Zhang, W.; Li, J.; Hui, L.; Feng, H. Atomic Layer Deposited Palladium Nanoparticle Catalysts Supported on Titanium Dioxide Modified MCM-41 for Selective Hydrogenation of Acetylene. *Appl. Surf. Sci.* **2019,** 495, 143495. DOI: 10.1016/J.APSUSC.2019.07.237.

(53) Chen, R.; Qu, K.; Li, J.; Zhu, P.; Duan, C.; Zhang, J.; Li, X.; Liu, X.; Yang, Z. Ultrathin Zirconia Passivation and Stabilization of Aluminum Nanoparticles for Energetic Nanomaterials via Atomic Layer Deposition. *ACS Appl. Nano Mater.* **2018**, *1* (10), 5500–5506. DOI: 10.1021/acsanm.8b01005.

(54) Park, J.; Lee, Y.; Chang, I.; Cho, G. Y.; Ji, S.; Lee, W.; Cha, S. W. Atomic Layer Deposition of Yttria-Stabilized Zirconia Thin Films for Enhanced Reactivity and Stability of Solid Oxide Fuel Cells. *Energy* **2016**, *116*, 170–176. DOI: 0.1016/J.ENERGY.2016.09.094.

(55) Oh, S.; Park, J.; Shin, J. W.; Yang, B. C.; Zhang, J.; Jang, D. Y.; An, J. High Performance Low-

Temperature Solid Oxide Fuel Cells with Atomic Layer Deposited-Yttria Stabilized Zirconia Embedded Thin Film Electrolyte. *J. Mater. Chem. A* **2018**, *6* (17), 7401–7408. DOI: 10.1039/C7TA10678E.

(56) Fan, L.; Zhu, B.; Su, P. C.; He, C. Nanomaterials and Technologies for Low Temperature Solid Oxide Fuel Cells: Recent Advances, Challenges and Opportunities. *Nano Energy* **2018**, 45, 148–176. DOI: 10.1016/j.nanoen.2017.12.044.

(57) Pessoa, R. S.; Fraga, M. A.; Chiappim, W.; Maciel, H. S. Exploring the Properties and Fuel Cell Applications of Ultrathin Atomic Layer Deposited Metal Oxide Films. *Emerg. Mater. Energy Convers. Storage*, Cheong, K.Y.; Impellizzeri, G.; Fraga, M.A.; Eds.;El Sevier, London, **2018**, 83–114. DOI: 10.1016/B978-0-12-813794-9.00003-X.

(58) Shim, J. H.; Chao, C. C.; Huango, H.; Prinz, F. B. Atomic Layer Deposition of Yttria-Stabilized Zirconia for Solid Oxide Fuel Cells. *Chem. Mater.* **2007**, *19* (15), 3850–3854. DOI: 10.1021/cm070913t.

(59) Shim, J. H.; Park, J. S.; An, J.; Gür, T. M.; Kang, S.; Prinz, F. B. Intermediate-Temperature Ceramic Fuel Cells with Thin Film Yttrium-Doped Barium Zirconate Electrolytes. *Chem. Mater.* **2009**, *21* (14), 3290–3296. DOI: 10.1021/cm900820p.

(60) Park, J. S.; Kim, Y. B.; Shim, J. H.; Kang, S.; Gür, T. M.; Prinz, F. B. Evidence of Proton Transport in Atomic Layer Deposited Yttria-Stabilized Zirconia Films. *Chem. Mater.* **2010**, *22* (18), 5366–5370. DOI: 10.1021/cm1017536.

(61) Konda, A.; Rau, A.; Stoller, M. A.; Taylor, J. M.; Salam, A.; Pribil, G. A.; Argyropoulos, C.; Morin, S. A. Soft Microreactors for the Deposition of Conductive Metallic Traces on Planar, Embossed, and Curved Surfaces. *Adv. Funct. Mater.* **2018**, *28* (40). DOI: 10.1002/ADFM.201803020.

(62) Tian, M.; Su, Y.; Zheng, H.; Pei, G.; Li, G.; Riffat, S. A Review on the Recent Research Progress in the Compound Parabolic Concentrator (CPC) for Solar Energy Applications. *Renew. Sustain. Energy Rev.* **2018**, *82*, 1272–1296. DOI: 10.1016/J.RSER.2017.09.050.

(63) Ko, H. C.; Stoykovich, M. P.; Song, J.; Malyarchuk, V.; Choi, W. M.; Yu, C. J.; Geddes, J. B.; Xiao, J.; Wang, S.; Huang, Y.; Rogers, J. A. A Hemispherical Electronic Eye Camera Based on Compressible Silicon Optoelectronics. *Nat.* **2008**, *454* (7205), 748–753. DOI: 10.1038/nature07113.

For Table of Contents Use Only

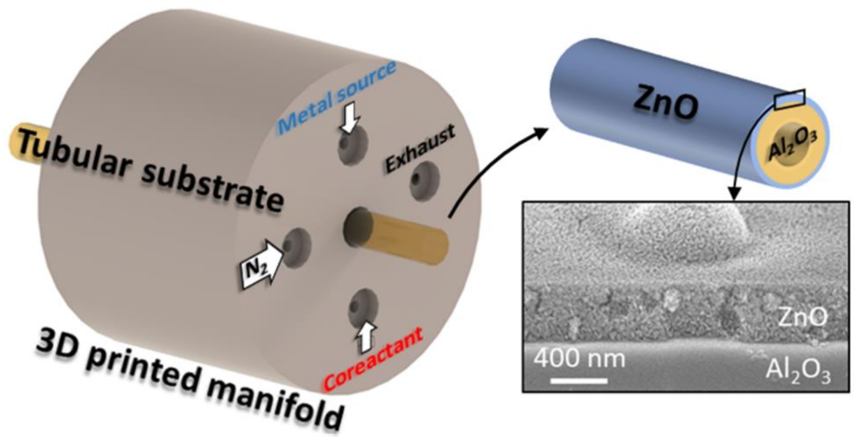

3D-printed spatial atomic layer deposition gas manifold for coating of non-planar substrates like tubular samples